Band-Engineered Bismuth Titanate Pyrochlores for Visible Light Photocatalysis

Sankaran Murugesan,[†] Muhammad N. Huda,[§,‡] Yanfa Yan,[‡] Mowafak M. Al-Jassim,[‡] and Vaidyanathan (Ravi) Subramanian*,[†]

Department of Chemical and Metallurgical Engineering, University of Nevada, Reno, Nevada 89557, and National Renewable Energy Laboratory, Golden, Colorado 80401

Received: July 2, 2009; Revised Manuscript Received: April 11, 2010

A density functional theory (DFT) study on stoichiometric bismuth titanate pyrochlore ($Bi_2Ti_2O_7$−BTO) is presented. Pseudopotential plane wave calculations were carried out to determine band gaps, density of states (DOS), and partial density of states (PDOS) of BTO. The theoretically determined optical property of BTO with a direct band gap of 2.6 eV corresponds to a red shift of 70 nm in absorption activity compared to titanium dioxide (TiO_2). A rationale has been developed to determine various possibilities of adding impurity elements within the BTO structure to enhance the visible light absorption. Mainly the effects of 3d element (Fe, Ni, Cr, Mn, and V) substitution in the crystal structure of BTO at the titanium position have been the focus of this study. The substitution of these elements shows the formation of different midgap states which indicates the flexibility of the BTO structure to tunability. Among the elements studied, Fe substitution showed a shift in the valence band toward the conduction band. This band gap reduction may facilitate a better electron transfer process. These theoretical results suggest that BTO can be a promising candidate for photocatalytic applications, such as solar-assisted water splitting reactions.

Introduction

Solar hydrogen production by water splitting is an environmentally benign method to produce energy. However, this method is challenging since solar hydrogen production is a relatively inefficient process compared to high-temperature hydrogen production from hydrocarbons. For the conversion of solar energy, there is a need to find an appropriate material that is photoactive in a broad spectrum of light and stable in electrolyte medium. Several photoactive materials for hydrogen production have been examined.[1–3] Photocatalysts, such as transition metal oxides (TiO_2, WO_3,[4] Fe_2O_3),[5–8] mixed oxides,[9–11] and chalgonides[12–14] have been primary candidates of interest. However, these photocatalysts have limitations such as harvesting only UV light (TiO_2), toxicity (CdSe), and instability issues (composites such as TiO_2−Au).[15–17] Binary metal oxides with different crystal structures show excellent photoactivity due to the orientation of atoms in a layer structure and the presence of vacancies in the crystal structure. For example, different crystal structures such as perovskites (ABO_3), pyrochlores ($A_2B_2O_7$), spinels (AB_2O_4), and delafossites (ABO_2) are of interest as photocatalysts. In this context, pyrochlores are a family of interesting compounds that can offer the properties desired of an ideal photocatalyst.[9,18–20] Generally, the pyrochlores can be represented as $A_2^{3+}B_2^{4+}O_7$ (or $A_2O{\cdot}B_2O_6$) which has an interpenetrating cuprite-type A_2O tetrahedral framework along with a corner sharing BO_6 octahedron.[21,22] Several elements can be used in the A site as well as in the B site to design a pyrochlore.

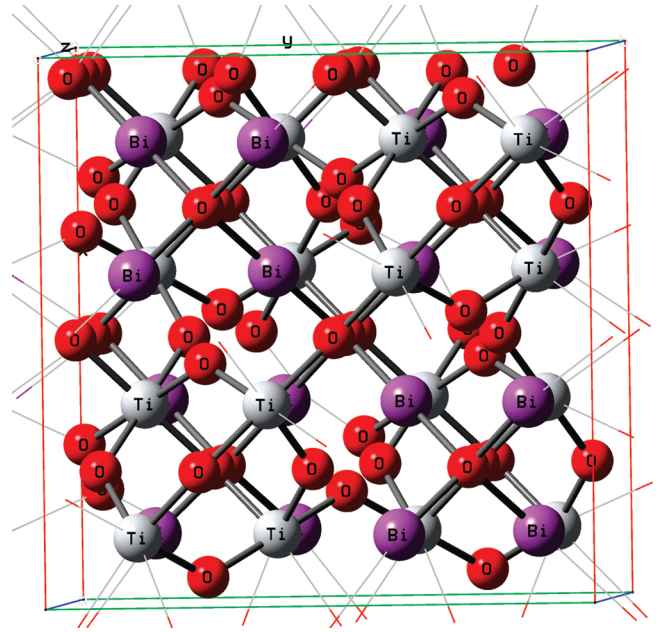

Figure 1. Crystal structure of bismuth titanate (BTO) of pyrochlore geometry ($Bi_2Ti_2O_7$) constructed for the theoretical study. (In the color diagram: the gray indicates Ti, red indicates oxygen, and purple indicates the Bi atom.)

From the photocatalytic point of view, pyrochlores are interesting as they offer the ability to manipulate electron/hole mobility by choice of different elements introduced in the structure.[23] Charge mobility can be one of the factors that controls the photocatalytic activity by influencing the probability of photogenerated charges reaching the reaction site of a photocatalyst.[24] The variation in the composition of A, B, and oxygen sites in $A_2B_2O_7$, as well as bond length variation, together contribute lone pair electrons which influence the electronic structure of pyrochlore.[22,25–27] The band structure and

* To whom correspondence should be addressed. Chemical & Metallurgical Engineering Department, Room 310, LMR 474, Mail stop 388, University of Nevada, Reno 89557. Phone: (775) 784 4686. Fax: (775) 327 5059. E-mail: ravisv@unr.edu.
[†] University of Nevada.
[‡] National Renewable Energy Laboratory.
[§] Present address: Physics Department, University of Texas, Arlington, TX, USA

10.1021/jp906252r
Published on Web 05/25/2010

TABLE 1: (a) Details of the BTO Pyrochlore Crystal Geometry and Symmetry Space Group Described and (b) Atomic Distance and Atomic Charge in BTO

(a)	
symmetry group	BTO original crystal
periodicity	3D (crystal)
name	FD-3M
international tables #	227
option	Origin-1
long name	F 41/D-32/M
Schoenfiles name	OH-7
crystal system	Cubic; $a = b = c = 10.2978$ Å; $\alpha = \beta = \gamma = 90°$
crystal class	m-3m
face-centered	(0,0,0), (0,1/2,1/2) (1/2,0,1/2), (1/2,1/2,0)
# of operators	192

(b) bond	population	length (Å)	experimental data[21]
$O_{(48f)}$−Ti	0.44	1.988	1.964
$O_{(8a)}$−Bi	0.16	2.229	2.227
$O_{(48f)}$−Bi	0.12	2.541	2.559

species	s	p	d	f	total	charge (e)
$O_{(8a)}$	1.87	4.89	0.00	0.00	6.76	−0.76
$O_{(48f)}$	1.90	5.04	0.00	0.00	6.95	−0.95
Ti	2.31	6.47	2.11	0.00	10.89	1.11
Bi	1.80	1.54	0.00	0.00	3.35	1.65

the mixing of orbitals to absorb visible light of the solar spectrum can be tuned by choice of elements from different groups of the Periodic Table.[23] This described property can be designed by choosing any element for introduction in the A and B sites as long as they satisfy the ratio $r_A/r_B = 1.29-2.30$ (r = ionic radius) and maintain an overall charge neutrality within the structure.[28–31]

Bismuth titanate in stoichiometric pyrochlore crystal structure exists as $Bi_2Ti_2O_7$. Bi occupies the A site with +3 oxidation state, and Ti occupies the B site with +4 oxidation state to form stoichiometric $A_2B_2O_7$ pyrochlore. In recent studies, the choice of bismuth as the element for the A site of the pyrochlore has been shown in photocatalysis.[32,33] Using a p-block element, such as bismuth, has been reported to show high electron mobility as well as improved photocatalytic activity compared with TiO_2.[34] In Bi, the 6s orbital helps to shift the valence band upward to reduce the band gap.[35] This phenomenon has also been shown in different crystal structures of BTO, especially in layered compounds of perovskite $Bi_4Ti_3O_{12}$[36–38] and sillenite $Bi_{12}TiO_{20}$.[39]

A general schematic representation of BTO pyrochlore band edges in comparison with TiO_2 band edges is shown in Figure S1 (Supporting Information). The structure of BTO pyrochlore can be written as $Bi_2Ti_2O_6O'$, where the oxygens are differentiated by 48f and 8a positions. Distortion in the TiO_6 octahedra causes the Ti t_{2g} orbitals to overlap with the 2p and 2s orbitals of oxygen. The 6s levels of Bi causes the formation of localized orbitals in the valence band (Ti−Oπ) and conduction band (Ti−Oπ* levels). Generally, the Bi^{3+} cation in the BTO pyrochlore structure shows a distorted Bi_2O' network.[22] This disorder is due to the static displacement, by the lone pair of electrons in the Bi^{3+} cation. Further, complex pyrochlores can also be prepared by suitable substitution of different group elements at the A and B sites. The structures are represented by a general formula $[A_xA'_{1-x}]_2B_2O_7$ $[(Fe_{0.2}Bi_{0.8})_2Ti_2O_7]$[40] or $A_2[B_xB'_{1-x}]_2O_7$ $[Bi_2MNbO_7$ (M = Al, Fe, In, Sm)].[41] Thus, multiple elements can be selected to be included at A and B sites to tailor the properties of the pyrochlore composite. Pyrochlores allow internal flexibility for different charge balanced combinations as well ($A_2^{3+}B_2^{4+}O_7$, $A_2^{2+}B_2^{5+}O_7$, and $A_2^{1+}B_2^{6+}O_7$).[42–44] However, from the perspective of solar energy harvesting for visible light photocatalysis, BTO in stoichiometric pyrochlore ($Bi_2Ti_2O_7$) crystal structure has not yet been examined. The effects of substitution in the BTO structure are also not well understood. A systematic study of bismuth titanate and substituted bismuth titanate pyrochlores is thus required.

In a recently published paper, different families of the Bi−Ti−O group have been studied along with nonmetal element (nitrogen and carbon) substitution. In the case of C and N doped BTO structures, the electronic properties depend on the extent of the impurity p-orbital mixing with the host valence band.[45] However, no systematic theoretical study has been found in the literature on transition metal substituted BTOs in spite of the fact that, in general, metal substitution can promote catalytic activity. Here, we report an in-depth analysis of the suitability of stoichiometric BTO pyrochlore for visible light photocatalytic activity through first-principle calculations. These studies examine the optical and electronic properties of BTO and 3d transition metal substituted BTO. The effect of these substitutions at the Ti site on band properties has been examined and compared with TiO_2. The optical properties of BTO and substituted BTO have been examined keeping in mind its applicability to the water redox property. These studies lay the foundations of a fundamental approach for examining and identifying appropriate photocatalysts with the right band gap for visible light activity.

Computational Model and Methodology

The first-principle computational calculations of BTO were performed by using the plane wave based DFT. The CASTEP program in Materials Studio supplied by Accelrys has been utilized in this study. Ultrasoft pseudopotentials were used with a plane wave basis set with a kinetic energy cutoff of 300 eV. We have considered a cutoff of 300 eV for various reasons. First, published reports have examined different cutoff energies from 250 to 400 eV for $In_xGa_{1-x}N$ utilizing a CASTEP code

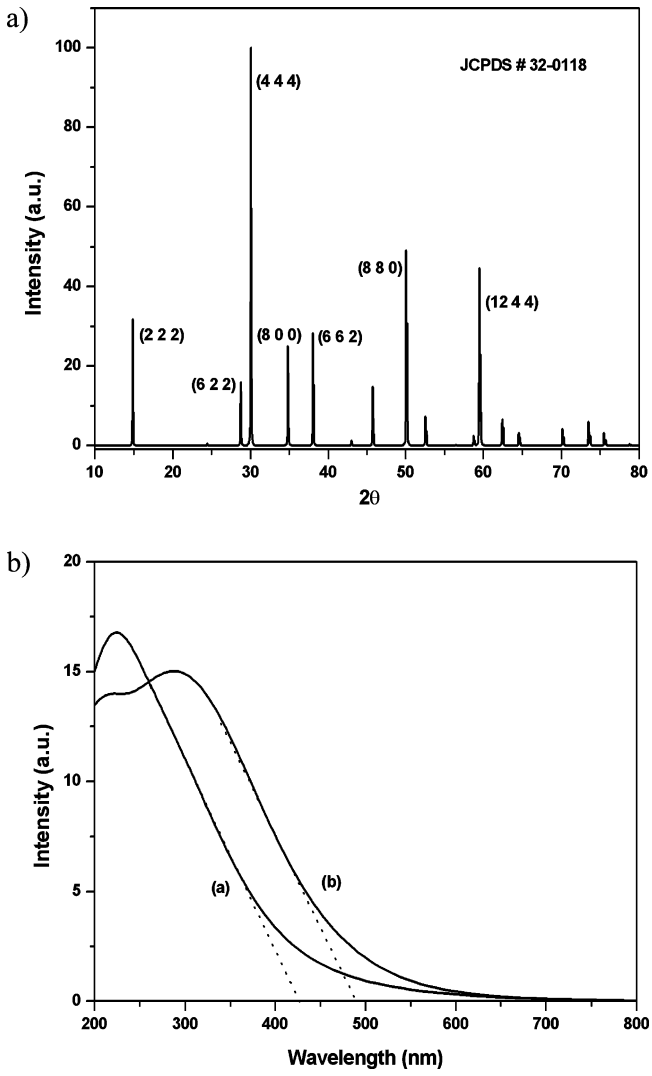

Figure 2. (a) XRD pattern of the BTO pyrochlore crystal structure simulated using density functional theory (DFT) calculations. The *hkl* values are indexed to the JCPDS file # 32-0118. (b) The simulated optical absorbance spectra of (a) TiO_2 anatase and (b) BTO with pyrochlore structure are shown. Note that the onset absorbance of BTO pyrochlore in (b) is located at 495 nm (red-shifted by 70 nm compared to TiO_2 at 425 nm).

similar to ours and concluded that 300 eV cutoff is an appropriate trade-off between accuracy and computational cost.[46] Another report on $Ga_{1-x}Zn_xN_{1-x}O_x$ compared plane wave cutoff energy at 340 and 300 eV, and these authors concluded that structural and electronic property changes are minimal at the two cutoffs.[47] Second, it is well-known that TiO_2 is a widely studied material for photoelectrodes. Therefore, it is imperative to compare the electronic properties of BTO with those of TiO_2 using the criteria used for TiO_2 in other studies. So, we have chosen a cutoff that has already been employed and verified for TiO_2. For example, there are studies available on TiO_2 with the same code as ours with 300 eV cutoff energy.[48,49] Finally, we have found that 300 eV cutoff energy produces reliable results for the density of states and optical properties of BTO (as evidenced from our previously published experimental paper with preliminary modeling information[50]). The Generalized Gradient Approximation (GGA) with Perdew−Wang exchange and correlation functional (PW91) has been adopted for the DFT calculations.[51,52] It is important to mention here that ref 45 uses a PBE functional.

BTO with a pyrochlore crystal structure (Figure 1) was considered for the computational study. The details of the symmetry space group, atomic population with individual s, p, d, and total charge on the species, and bond length of optimized crystal are given in Table 1. BTO with a pyrochlore crystal structure was obtained from the Inorganic Crystal Structure Database (ICSD) (ICSD# 413013) for verifying the computational output.[22] All the properties have been calculated by utilizing a primitive unit cell of the BTO pyrochlore crystal structure. The symmetry of crystal structure was automatically reduced to point symmetry operators without transitional components. All electronic band structures and the optical absorption spectra were calculated on the corresponding optimized crystal geometries with $3 \times 3 \times 3$ k-point sampling using Monkhorst-Pack grid parameters. The scissors operator has not been considered in these calculations. All the structures are optimized with a convergence accuracy of 5×10^{-5} eV/atom. The atomic coordinates are obtained by minimizing total energy as well as atomic forces. The cell parameters had been optimized along with atomic coordinates during the iterative optimization. The magnetic moments of the atoms were also not considered in the calculation. Reflex Tool in Materials Studio software was used to find the XRD pattern of optimized crystals in the polycrystalline mode. Anatase TiO_2 (ICSD # 82080) was considered as a standard for comparison.

Results and Discussions

1. XRD and Optical Absorption Property. The crystal structure used to study the electronic properties was subject to theoretical simulation of powder XRD pattern in the polycrystalline mode. The DFT powder X-ray diffraction was determined over the 2θ range from 5 to 80°. The X-ray radiation source was Cu Kα with a wavelength $\lambda = 1.54439$. Figure 2a shows the XRD pattern for the BTO crystal obtained from theoretical simulations. The peaks obtained in the calculation were identified and indexed to $Bi_2Ti_2O_7$ (JCPDS # 32-0118) value. The 100% peak at $2\theta = 29.99$ corresponds to the (444) *hkl* plane; $2\theta = 28.7$ corresponds to the (622) plane; and $2\theta = 14.89$ corresponds to the (222) plane. From this analysis, it can be inferred that the crystal structure obtained from the theoretical calculations shows the XRD pattern similar to experimentally synthesized $Bi_2Ti_2O_7$. Since the XRD pattern of the simulated BTO matches well with the experimental values for a crystalline BTO pyrochlore, it suggests that the model crystal structure used for DFT calculations is in pyrochlore crystal geometry. Similarly, the XRD pattern for anatase TiO_2 crystal obtained using the simulation is given in Figure S2 (Supporting Information). This XRD shows the peaks that correspond to anatase TiO_2 with JCPDS # 21-1272.

The next task was to simulate the optical response of BTO and determine its light absorbance. The geometrically optimized crystal structure was considered for studying the optical properties. To calculate the optical absorbance, the polycrystalline BTO pyrochlore crystal was used with a smearing of 0.5 eV. A similar kind of approach was adopted for TiO_2 crystal in previous literature.[53–55] Absorption spectra are generated as a plot of absorption intensity with respect to the wavelength (nm). The optical property of BTO was compared with TiO_2 adopting a similar computational procedure. Figure 2b shows the DFT generated absorption spectra of BTO pyrochlore and TiO_2. The visible light activity of the BTO is evident from the red shift in the onset of absorbance compared to TiO_2. The estimated onset absorbance of TiO_2 is 425 nm, while that of BTO is 495 nm. It can be noted that BTO demonstrates both

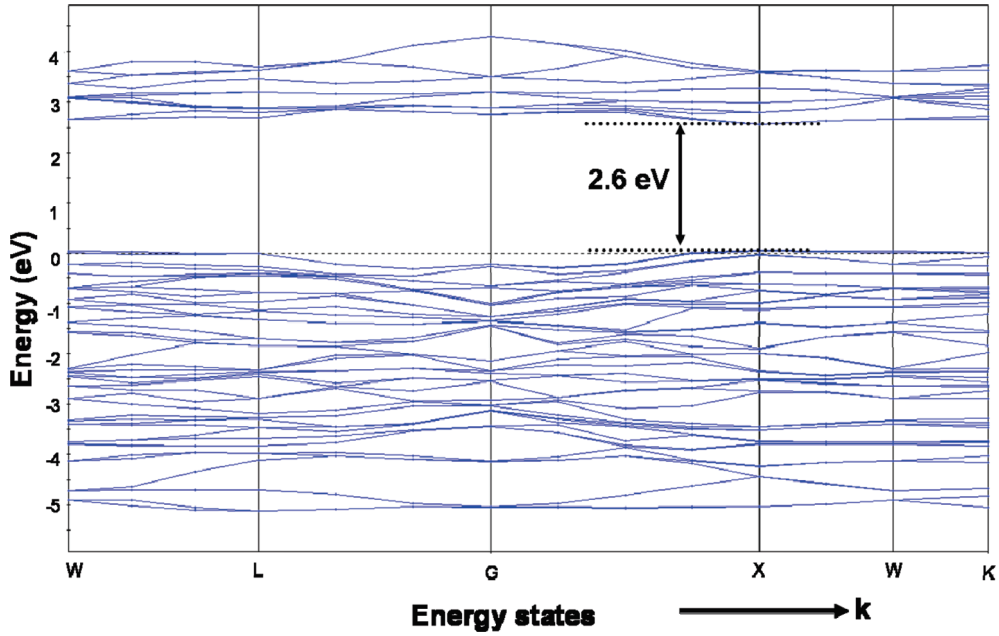

Figure 3. Electronic band diagram of the BTO pyrochlore crystal along the k-vector.

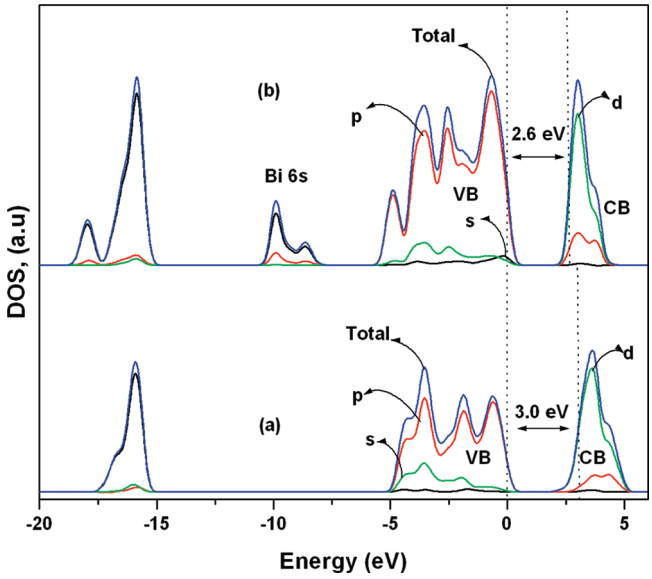

Figure 4. Comparison of total density of states of (a) TiO_2 and (b) BTO pyrochlore, where BTO shows contribution from 6s orbitals of Bi in the valence band.

UV light absorption property similar to TiO_2 and visible light absorption due to the red shift in absorption edges. The shift of 70 nm shows the visible light absorption by the BTO. Generally, substitution or doping of the TiO_2 crystal shows visible light activity but at losses of UV activity.[56–58] This simulation suggests that BTO visible light activity, with no loss of UV activity, can be advantageous and lead to an overall enhancement in light absorption

2. DOS and Band Gap Variation. Figure 3 shows the band diagram of BTO. The k-vector along the symmetry lines of the first Brilliouin-zone was examined. In the band diagram, a clear separation of valence band and conduction band with a gap of 2.6 eV was noticed along the Brilliouin-zones of W, L, X, and K. This can be attributed to the unique structure of the pyrochlore which allows for element-specific varying degree of hybridization to occur. The band structure across the various high symmetry directions is consistent with the electronic band gap noted in the calculation. For TiO_2, theoretical calculations and experimental results have shown an indirect band gap of 3.2 eV.[59,60] The alignment of the valence band (VB) maxima and conduction band (CB) minima toward the same k-vector, shown in Figure 3, suggests that the $Bi_2Ti_2O_7$ is a direct band gap material, and the minimum gap was found at the X-point. Similar observations have been noted for $Ca_2Nb_2O_7$ and $Ca_2Ta_2O_7$ in pyrochlores.[61] In contrast, the recently published JPCC paper mentioned an indirect gap of 2.46 eV for pyrochlore BTO.[45] However, their reported band gap at Γ-point, 2.89 eV, is similar to the band gap we found from our calculations at the Γ-point in Figure 3. The direct band gap materials are likely to be more efficient in a photocatalytic process as they promote minimization of recombination losses due to trapping of the excited electrons as they transit from the valence band to the conduction band. This shows that BTO will be useful for photocatalytic applications. Generally, in metal oxides, the VB is formed by the oxygen 2p orbitals in TiO_6 octahedra, while CB is formed by the d orbitals associated with the metal occupying the B site.[62]

The partial density of states (PDOS) of BTO was also analyzed. BTO shows a reduced band gap of 0.4 eV compared to TiO_2 (Figure 4) in the total density of states. This provides a quantitative estimate of the extent of band gap reduction. There is a clear and distinct peak formation noticed in the energy range between −8.0 and −11 eV. The presence of an interband in the valence band of BTO is due to the contribution from the 6s orbitals of the Bi atom. Thus, the combination of oxygen 2p orbitals and 6s orbital of BTO contributes to the reduction of the band gap. The interband formed by the occupied Bi 6s orbitals shifts the valence band toward the conduction band, which, in turn, leads to visible light activity and assists with a facile electron transfer process.

3. Analysis of Conduction Band. The characteristics of the conduction band are an important parameter to be evaluated in studying the efficiency of the photocatalytic process. These studies also help identify methods to avoid recombination loss and favor competent electron transfer processes. In the case of BTO pyrochlore, the conduction band is mainly derived from the 3d bands of the Ti atom along with an additional contribution

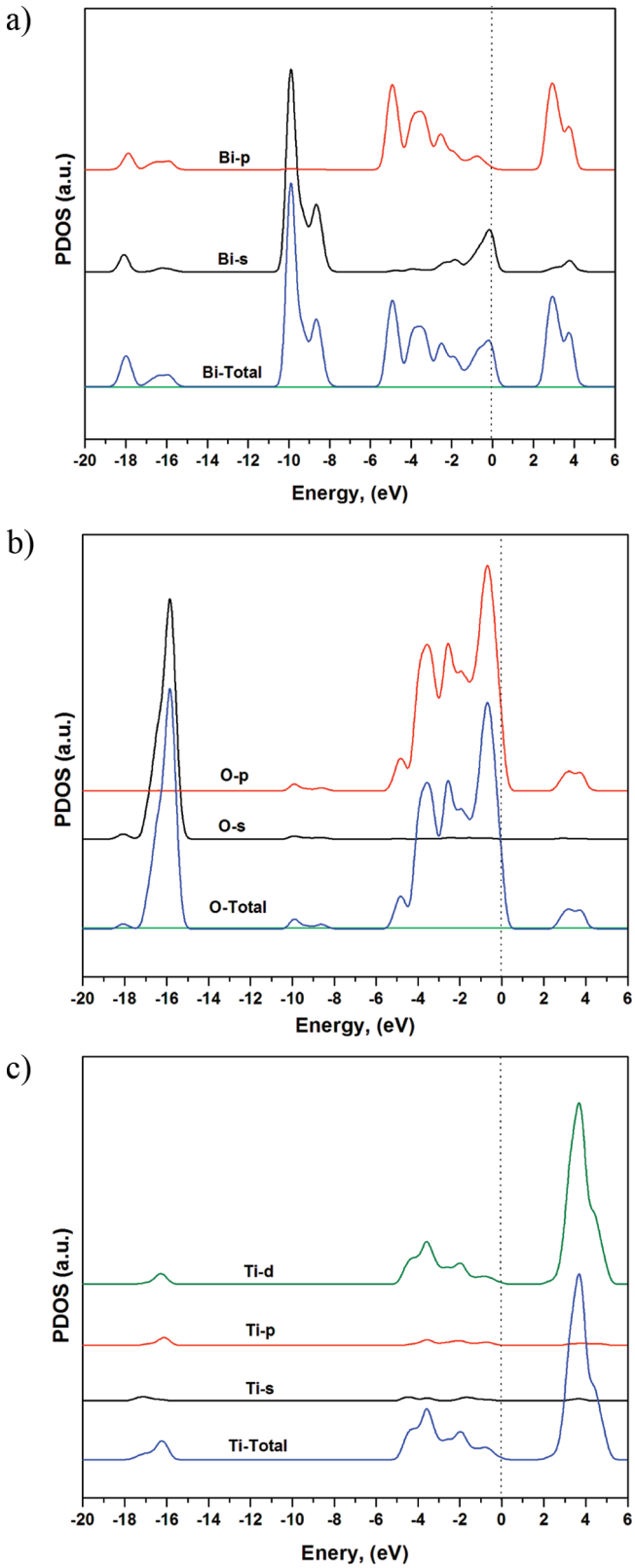

Figure 5. Partial density of states (PDOS) of each element (a) Bi p, Bi s, (b) Ti d, Ti p, Ti s, and (c) O p, O s that forms the BTO structure and the sum total of all orbital contributions for each element.

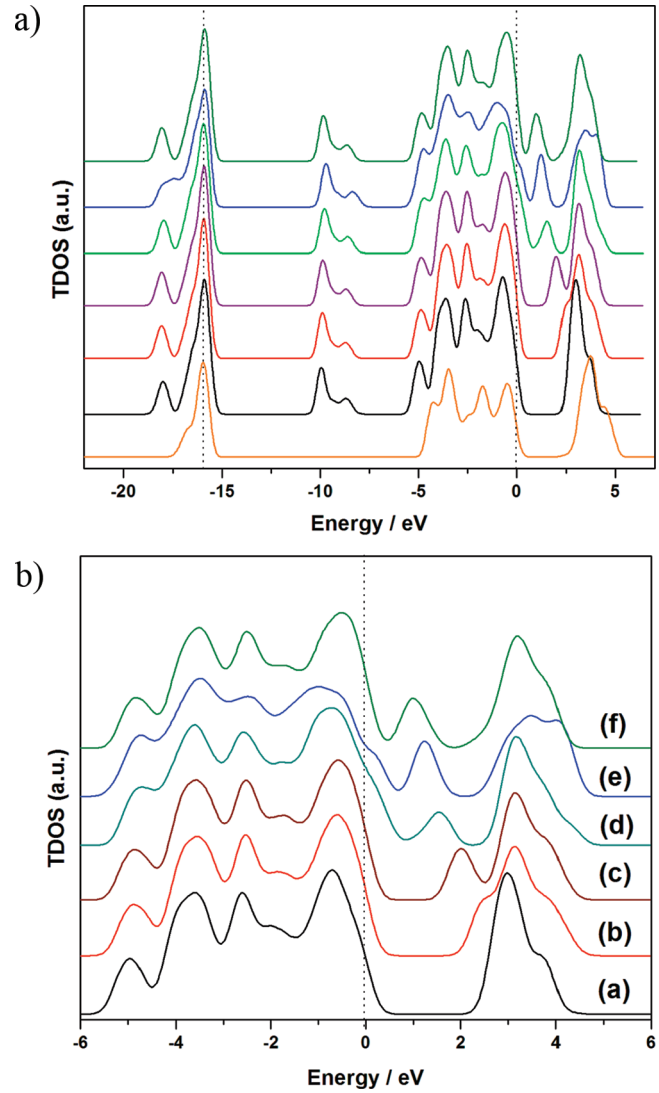

Figure 6. (a) TDOS of BTO after substitution of 3d elements at the Ti site and aligning with respect to oxygen deep level orbitals in comparison to TiO_2: (a) TiO_2, (b) $Bi_2Ti_2O_7$, (c) $Bi_2Ti_{1.5}V_{0.5}O_7$, (d) $Bi_2Ti_{1.5}Cr_{0.5}O_7$, (e) $Bi_2Ti_{1.5}Ni_{0.5}O_7$, (f) $Bi_2Ti_{1.5}Mn_{0.5}O_7$, (g) $Bi_2Ti_{1.5}Fe_{0.5}O_7$. (b) The variation of TDOS due to 3d-element substitution at the Ti site in the BTO crystal structure in comparison to TiO_2 shown over the range −6 to +6 eV: (a) TiO_2, (b) $Bi_2Ti_2O_7$, (c) $Bi_2Ti_{1.5}V_{0.5}O_7$, (d) $Bi_2Ti_{1.5}Cr_{0.5}O_7$, (e) $Bi_2Ti_{1.5}Ni_{0.5}O_7$, (f) $Bi_2Ti_{1.5}Mn_{0.5}O_7$, and (g) $Bi_2Ti_{1.5}Fe_{0.5}O_7$.

from the p-band of the Bi atom. In photochemical reactions, the stability of the electrons in the conduction band helps in reduction of recombination rates of excited charges. Since the valence band mainly consists of oxygen p-orbitals, it will be useful to have more p-character in the conduction band to avoid recombination. Since Bi contributes the p-character of BTO, we further examined the CB in detail. Figure 5 shows the partial density of states (or PDOS) of individual elements in BTO. It is noted that the contribution of the s orbital from Bi plays an important role. The shift in the conduction band of BTO is due to the combined effect of empty d-orbitals of the Ti atom and Bi 6p states. To find the percentage of p-character in the conduction band, the partial density of states (PDOS) was calculated. The analysis indicates that the percentage of the p-character increased in BTO by 7% (from 14.32% in TiO_2 to 21.68% in BTO). This shows that the presence of Bi in the A site helps not only to shift the VB but also to enhance synchronized mixing of the p-orbital in the CB which in turn can improve the electron transfer process.

4. Effect of Substitution. Addition or substitution of transition metal atoms like Fe, Cr, Mn, and Ni and also nonmetallic elements, such as nitrogen, sulfur, and carbon, in the TiO_2 structure, are reported to have increased photocatalytic activity.[63,64] Especially, substitution of transition metals in TiO_2 shows visible

SCHEME 1: List of Elements That Fit the General Formula $Bi_2Ti_{1-x}M_xO_7$ (Where M = Element Which Can Be Substituted at the Ti Site)[a]

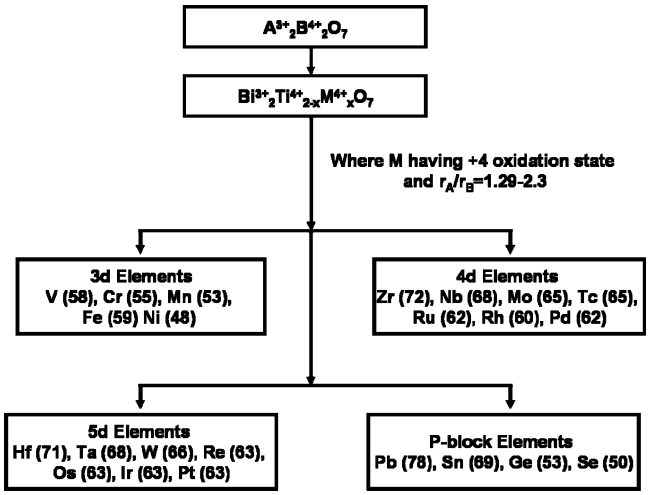

[a] Essential criteria for the stable pyrochlore formation are r_A/r_B = 1.29−2.30 (r = ionic radius) and the overall charge neutrality. The numbers in the brackets are ionic radius of the element in picometers.

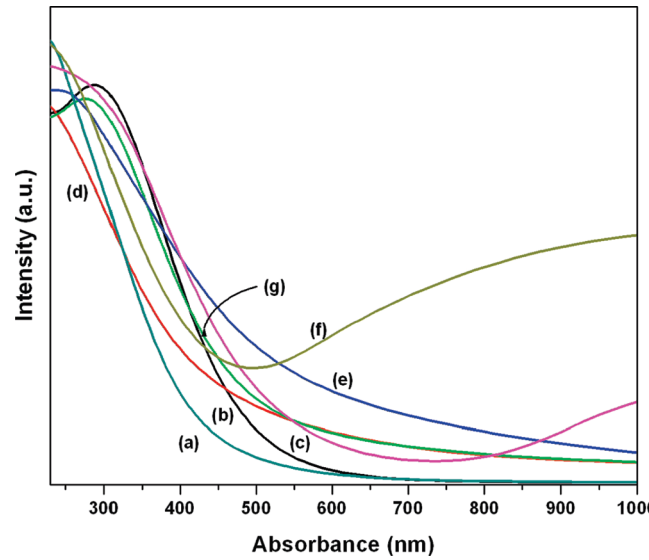

Figure 7. Comparison of DFT simulated optical spectra of TiO_2 anatase and various 3d transition element substituted BTO pyrochlore crystal: (a) TiO_2, (b) $Bi_2Ti_2O_7$, (c) $Bi_2Ti_{1.5}V_{0.5}O_7$, (d) $Bi_2Ti_{1.5}Cr_{0.5}O_7$, (e) $Bi_2Ti_{1.5}Ni_{0.5}O_7$, (f) $Bi_2Ti_{1.5}Mn_{0.5}O_7$, and (g) Bi_2 $Ti_{1.5}Fe_{0.5}O_7$.

light activity, and each element behaves differently when substituted into the TiO_2 lattice. BTO structure has the ability to accommodate a variety of elements which can satisfy the charge neutrality and the ionic radii requirements. Different elements can be substituted in the A and B sites of the bismuth titanate pyrochlore. The Bi atom is essential at the A site to enhance the visible light absorption activity by shifting the valence band toward the conduction band in BTO. Therefore, we discuss the effect of substitution at the B site (Ti atom) with +4 oxidation state elements. It was shown that a change at the B site of the pyrochlore can affect CB and VB properties, such as orbital mixing, charge transport, and band edge locations.[24,65] Such compounds are represented by the general formula $Bi_2Ti_{2-x}M_xO_7$ (M = substituted element at the Ti site). Besides, there also exists the possibility of a substitution of a trivalent (M^{3+}) or a pentavalent (M^{5+}) cation in the B site.[42–44] In this paper, the substitution of various transition metals of the tetravalent cation (M^{4+}) in the Ti^{4+} position is considered. A list of suitable elements for substitution at the Ti site from different blocks is identified in Scheme 1. Elements that demonstrate a +4 oxidation state and that meet the charge neutrality requirement (ionic radii ratio r_A/r_B = 1.29−2.30 (r = ionic radius)) are identified as compatible within the BTO structure.

Among the type of elements that can be substituted at the Ti site, 3d elements demonstrate the most interesting behavior that includes manipulation of visible light activity as well as tuning of interband state locations.[66–68] 3d elements generally tend to form octahedral crystal structure, in which they exhibit split states of d-orbitals in the form of t_{2g} and e_g levels in the higher energy region. As the number of 3d electrons increases, both t_{2g} and e_g states shift to the lower energy because the positive nuclear charge increases with this change. This change makes the chemical potential of d-electrons lower and closer to the p-orbital.[66–68] It is, therefore, of interest to study the effect of 3d elements on the BTO crystal structure. Theoretical calculations were carried out by substituting 3d elements (Fe, Ni, Mn, Cr, and V) given in Scheme 1. About 25% of the Ti site in the optimized BTO crystal structure was considered for substitution by 3d elements. The substitution of x = 0.25 was arbitrarily chosen. This relatively higher impurity level was chosen so that a systematic study can be made with the 3d transition metal element substitutions with reasonable computing time. We believe that the results may vary with reduction in doping level; however, the trends are not expected to change significantly. In addition, the fraction experimentally noted for the formation of stable substituted photoactive pyrochlores lies over a much broader range ($Bi_2Ti_{2-x}M_xO_7$, where x = 0−1), and the results presented here are representative within this range. The substitution position of 3d elements in the BTO crystal structure is shown in Figure S3 (Supporting Information). Figure 6a shows the aligned TDOS plots of various substituted 3d metals of BTO in comparison to TiO_2. The Fermi level of all the substitutions has been aligned with respect to the deep oxygen orbital energy levels. For a clear understanding of Fermi level alteration with respect to 3d transition metal substitution in BTO, Figure 6a was expanded in the region of interest between 6 and −6 eV in Figure 6b. This analysis shows that 3d transition metal substitution in the BTO structure shows variation in Fermi levels by forming substrates between the VB and CB. Formation of such sub- or interband states can be noticed with substitution of any element from the group. A shift in the valence state with the nature of the substituted 3d element is also observed. This formation of interband states can promote the charge transfer process efficiently as noted with 3d transition element doping in TiO_2.[66]

In a related study, a correlation between bandgap, ionic radii, and photoactivity was made for Bi_2RNbO_7 (R = Y and rare earth elements) for photocatalytic water splitting.[69] The study reports that as the ionic radii increase the bandgap increases causing a decrease in the photoactivity. When 3d elements are substituted in the BTO lattice, it results in band gap reduction due to the formation of midband states. Our analysis offers a choice of elements to be considered for substitution at the B site. The optical property of substituted BTO was identified to calculate the shift in the absorption activity. Figure 7 shows the optical property of 3d metal-substituted BTO. A shift in the onset absorption of BTO with substitution of 3d element atoms at the B site is evident. From the DOS analysis (Figure 6), it can be observed that substitution using any 3d element leads to the formation of midbands. These midbands are due to

the localized d-orbitals of 3d-metals. These midcenters may or may not increase the electron transfer process and depend upon the interaction with valence band or conduction band orbitals. Among these 3d elements, the substitution of Fe in BTO shows a band which is close to the valence band and is particularly interesting. This has the preferential probability to combine with the valence band to enhance the electron transfer process. It has been shown in the literature that, among different metals substituted (Fe, In, and Ga) for Ta in $Bi_2Ta_2O_7$, Fe has been noted to cause the least distortion of the $Bi_2Ta_2O_7$ structure and, hence, is believed to offer maximum stability.[9,41,70–72] Substitution of Fe shows a shift toward CB from VB, whereas other elements show a shift from the CB toward VB. Though midband formation plays a role in the reduction of the band gap, these can also act as recombination centers in case they are very localized. These results indicate the applicability of BTO as a possible candidate to tailor photocatalysts for energy conversion applications. The effects of substitute concentration and further detailed analysis of oxidation state through theoretical core shell spectroscopy and the nonstoichiometric composition analysis are needed to completely understand the full potential of these materials.

Conclusions

First-principle theoretical calculations of BTO support the possibility that BTO can be used in visible light photocatalytic applications for energy conversion. The effects of substitution of various 3d elements at the Ti site of the BTO on its optical and electronic properties have also been examined. Especially, formation of midband states by substitution of Fe in the pyrochlore structure leads to a shift in valence band toward the conduction band which enables reduction of the band gap. Utilization of these materials for photocatalysis depends upon development of simple and efficient synthesis methods. This study opens new approaches to identify unique blends of photoactive pyrochlores that might find applications in photocatalytic water splitting and photovoltaic materials that are active in visible light.

Acknowledgment. This work was performed with the funding provided by the University of Nevada, Reno Office, of the Vice President for Research as a part of a junior faculty startup package and an internal competitive junior faculty research grant. V.S. thanks the Office of Vice-President for Research for the funding. The work of M.N.H., Y.Y., and M.M.A. was supported by the U.S. Department of Energy under Contract # DE-AC36-08GO28308. The authors thank the reviewers for valuable insights on this work.

Supporting Information Available: Figures S1−S3. This material is available free of charge via the Internet at http://pubs.acs.org.

References and Notes

(1) Osterloh, F. E. Inorganic materials as catalysts for photochemical splitting of water. *Chem. Mater.* **2008**, *20* (1), 35–54.

(2) Meyer, T. J. Catalysis - The art of splitting water. *Nature* **2008**, *451* (7180), 778–779.

(3) Matsuoka, M.; Kitano, M.; Takeuchi, M.; Tsujimaru, K.; Anpo, M.; Thomas, J. M. Photocatalysis for new energy production - Recent advances in photocatalytic water splitting reactions for hydrogen production. *Catal. Today* **2007**, *122* (1−2), 51–61.

(4) Huda, M. N.; Yan, Y.; Moon, C.-Y.; Wei, S. H.; Al-Jassim, M. M. Physical Review B, 195102 (2008). Density funcitonal theory study of the effects of atomic impurity on the band edges of monoclinic WO3. *Phys. Rev. B* **2008**, *77* (19), 195102-1−195102-13.

(5) Hu, Y. S.; Kleiman-Shwarsctein, A.; Forman, A. J.; Hazen, D.; Park, J. N.; McFarland, E. W. Pt-doped alpha-Fe2O3 thin films active for photoelectrochemical water splitting. *Chem. Mater.* **2008**, *20* (12), 3803–3805.

(6) Nowotny, J.; Bak, T.; Nowotny, M. K.; Sheppard, L. R. TiO2 surface active sites for water splitting. *J. Phys. Chem. B* **2006**, *110* (37), 18492–18495.

(7) Galinska, A.; Walendziewski, J. Photocatalytic water splitting over Pt-TiO2 in the presence of sacrificial reagents. *Energy Fuels* **2005**, *19* (3), 1143–1147.

(8) Gondal, M. A.; Hameed, A.; Yamani, Z. H. Laser induced photocatalytic splitting of water over WO3 catalyst. *Energy Sources* **2005**, *27* (12), 1151–1165.

(9) Wang, J. H.; Zou, Z. G.; Ye, J. H. Synthesis, structure and photocatalytic property of a new hydrogen evolving photocatalyst Bi2InTaO7. *Funct. Graded Mater. Vii* **2003**, *42−34*, 485–490.

(10) Luan, J. F.; Hao, X. P.; Zheng, S. R.; Luan, G. Y.; Wu, X. S. Structural, photophysical and photocatalytic properties of Bi2MTaO7 (M = La and Y). *J. Mater. Sci.* **2006**, *41* (23), 8001–8012.

(11) Kako, T.; Kikugawa, N.; Ye, J. Photocatalytic activities of AgSbO3 under visible light irradiation. *Catal. Today* **2008**, *131* (1−4), 197–202.

(12) Babu, K. S.; Pandey, R. N.; Srivastava, O. N. Photoelectrochemical Semiconductor Septum (Cdse/Ti and Tio2/Ti) Solar-Cells in Relation to Hydrogen-Production. *Int. J. Hydrogen Energy* **1995**, *20* (10), 771–775.

(13) Frame, F. A.; Carroll, E. C.; Larsen, D. S.; Sarahan, M.; Browning, N. D.; Osterloh, F. E. First demonstration of CdSe as a photocatalyst for hydrogen evolution from water under UV and visible light. *Chem. Commun.* **2008**, (19), 2206–2208.

(14) Pandey, R. N.; Misra, M.; Srivastava, O. N. Solar hydrogen production using semiconductor septum (n-CdSe/Ti and n-TiO2/Ti) electrode based photoelectrochemical solar cells. *Int. J. Hydrogen Energy* **1998**, *23* (10), 861–865.

(15) Subramanian, V.; Wolf, E.; Kamat, P. V. Semiconductor-metal composite nanostructures. To what extent do metal nanoparticles improve the photocatalytic activity of TiO2 films. *J. Phys. Chem. B* **2001**, *105* (46), 11439–11446.

(16) Subramanian, V.; Wolf, E. E.; Kamat, P. V. Influence of metal/metal ion concentration on the photocatalytic activity of TiO2-Au composite nanoparticles. *Langmuir* **2003**, *19* (2), 469–474.

(17) Subramanian, V.; Wolf, E. E.; Kamat, P. V. Catalysis with TiO2/gold nanocomposites. Effect of metal particle size on the Fermi level equilibration. *J. Am. Chem. Soc.* **2004**, *126* (15), 4943–4950.

(18) Zeng, J.; Wang, H.; Zhang, Y. C.; Zhu, M. K.; Yan, H. Hydrothermal synthesis and photocatalytic properties of pyrochlore La2Sn2O7 nanocubes. *J. Phys. Chem. C* **2007**, *111* (32), 11879–11887.

(19) Abe, R.; Higashi, M.; Zou, Z. G.; Sayama, K.; Abe, Y. Photocatalytic water splitting into H-2 and O-2 over R2Ti2O7 (R = Y, rare earth) with pyrochlore structure. *Chem. Lett.* **2004**, *33* (8), 954–955.

(20) Ikeda, S.; Itani, T.; Nango, K.; Matsumura, M. Overall water splitting on tungsten-based photocatalysts with defect pyrochlore structure. *Catal. Lett.* **2004**, *98* (4), 229–233.

(21) Subramanian, M. A.; Aravamudan, G.; Rao, G. V. S. Oxide Pyrochlores - a Review. *Prog. Solid State Chem.* **1983**, *15* (2), 55–143.

(22) Hector, A. L.; Wiggin, S. B. Synthesis and structural study of stoichiometric BiTi2O7 pyrochlore. *J. Solid State Chem.* **2004**, *177* (1), 139–145.

(23) Kudo, A.; Kato, H.; Nakagawa, S. Water splitting into H-2 and O-2 on new Sr2M2O7 (M = Nb and Ta) photocatalysts with layered perovskite structures: Factors affecting the photocatalytic activity. *J. Phys. Chem. B* **2000**, *104* (3), 571–575.

(24) Campet, G.; Jakani, M.; Doumerc, J. P.; Claverie, J.; Hagenmuller, P. Photoconduction Mechanisms in Titanium and Rare-Earth N-Type Semiconducting Electrodes with Pyrochlore and Perovskite Structures. *Solid State Commun.* **1982**, *42* (2), 93–96.

(25) Tuller, H. L. Mixed Ionic Electronic Conduction in a Number of Fluorite and Pyrochlore Compounds. *Solid State Ionics* **1992**, *52* (1−3), 135–146.

(26) Pontonnier, L.; Fruchart, D.; Fournier, T.; Vaillant, F. Relationships between Structural and Electric Properties of Pure and Mixed Protonic Conductors. *Solid State Ionics* **1990**, *37* (4), 307–316.

(27) Vandijk, M. P.; Burggraaf, A. J.; Cormack, A. N.; Catlow, C. R. A. Defect Structures and Migration Mechanisms in Oxide Pyrochlores. *Solid State Ionics* **1985**, *17* (2), 159–167.

(28) Shannon, R. D. Revised Effective Ionic-Radii and Systematic Studies of Interatomic Distances in Halides and Chalcogenides. *Acta Crystallogr., Sect. A* **1976**, *32* (Sep1), 751–767.

(29) Shannon, R. D.; Prewitt, C. T. Revised Values of Effective Ionic Radii. *Acta Crystallogr., Sect. B: Struct. Crystallogr. Cryst. Chem.* **1970**, *B 26*, 1046.

(30) Shannon, R. D.; Prewitt, C. T. Derivation and Use of Effective Ionic Radii in Crystal Chemistry. *Am. Ceram. Soc. Bull.* **1968**, *47* (4), 366.

(31) Shannon, R. D.; Prewitt, C. T. Effective Ionic Radii in Oxides and Fluorides. *Acta Crystallogr., Sect. B: Struct. Crystallogr. Cryst. Chem.* **1969**, *B 25*, 925–&.

(32) Kudo, A.; Hijii, S. H-2 or O-2 evolution from aqueous solutions on layered oxide photocatalysts consisting of Bi3+ with 6s(2) configuration and d(0) transition metal ions. *Chem. Lett.* **1999**, (10), 1103–1104.

(33) Kako, T.; Zou, Z.; Ye, J. Photocatalytic oxidation of 2-propanol in the gas phase over cesium bismuth niobates under visible light irradiation. *Res. Chem. Intermed.* **2005**, *31* (4−6), 359–364.

(34) Ikarashi, K.; Sato, J.; Kobayashi, H.; Saito, N.; Nishiyama, H.; Inoue, Y. Photocatalysis for water decomposition by RuO2-dispersed ZnGa2O4 with d(10) configuration. *J. Phys. Chem. B* **2002**, *106* (35), 9048–9053.

(35) Walsh, A.; Yan, Y.; Huda, M. N.; Al-Jassim, M.; Wei, S.-H. Band edge electronic structure of BiVO4: Elucidating the role of the Bi s and V d orbitals. *Chem. Mater.* **2009**, *21*, 547–551.

(36) Vehkamaki, M.; Hatanpaa, T.; Kemell, M.; Ritala, M.; Leskelaa, M. Atomic layer deposition of ferroelectric bismuth titanate Bi4Ti3O12 thin films. *Chem. Mater.* **2006**, *18* (16), 3883–3888.

(37) Tada, M.; Osada, M.; Kakihana, M.; Noguchi, Y.; Miyayama, M. Photoconducting properties in oxygen-deficient Bi4Ti3O12. *Electroceram. Jpn. Viii* **2005**, *301*, 7–10.

(38) Pintilie, L.; Pintilie, I.; Alexe, M. Photoconductive properties of Bi4Ti3O12/Si heterostructures with different thickness of the Bi4Ti3O12 film. *J. Eur. Ceram. Soc.* **1999**, *19* (6−7), 1473–1476.

(39) Zhou, J. K.; Zou, Z. G.; Ray, A. K.; Zhao, X. S. Preparation and characterization of polycrystalline bismuth titanate Bi12TiO20 and its photocatalytic properties under visible light irradiation. *Ind. Eng. Chem. Res.* **2007**, *46* (3), 745–749.

(40) Yao, W. F.; Wang, H.; Xu, X. H.; Zhou, J. T.; Yang, X. N.; Zhang, Y.; Shang, S. X. Photocatalytic property of bismuth titanate Bi2Ti2O7. *Appl. Catal., A* **2004**, *259* (1), 29–33.

(41) Garza-Tovar, L. L.; Torres-Martinez, L. M.; Rodriguez, D. B.; Gomez, R.; del Angel, G. Photocatalytic degradation of methylene blue on Bi2MNbO7 (M = Al, Fe, In, Sm) sol-gel catalysts. *J. Mol. Catal. A: Chem.* **2006**, *247* (1−2), 283–290.

(42) Kim, S. S.; Kim, W. J. Electrical properties of sol-gel derived pyrochlore-type bismuth magnesium niobate Bi-2(Mg1/3Nb2/3)(2)O-7 thin films. *J. Cryst. Growth* **2005**, *281* (2−4), 432–439.

(43) Park, J. K.; Kim, C. H.; Choi, K. J.; Park, H. D.; Choi, S. Y. Photoluminescence behavior of Al3+, Pr3+ doped perovskite La2/3TiO3 and pyrochlore La2Ti2O7. *J. Mater. Res.* **2001**, *16* (9), 2568–2571.

(44) Sohn, J. M.; Kim, M. R.; Woo, S. I. The catalytic activity and surface characterization of Ln(2)B(2)O(7) (Ln = Sm, Eu, Gd and Tb; B = Ti or Zr) with pyrochlore structure as novel CH4 combustion catalyst. *Catal. Today* **2003**, *83* (1−4), 289–297.

(45) Wei, W.; Dai, Y.; Huang, B. First-principles characterization of Bi-based photocatalysts: Bi12TiO20, Bi2Ti2O7, Bi4Ti2O12. *J. Phys. Chem. C* **2009**, *113* (14), 5658–5663.

(46) Kuo, Y. K.; Chu, H. Y.; Yen, S. H.; Liou, B. T.; Chen, M. L. Bowing parameter of zinc blende InxGa1-xN. *Opt. Commun.* **2008**, *280* (1), 153–156.

(47) Wei, W.; Dai, Y.; Yang, K.; Guo, M.; Huang, B. Origin of the visible light absorption of GaN-rich Ga1-xZnxN1-xOx (x = 0.125) solid solution. *J. Phys. Chem. C* **2008**, *112* (40), 15915–15919.

(48) Tian, F.; Liu, C. DFT description of electronic strucuture and optical absorption properties of anionic S-doped anatase TiO2. *J. Phys. Chem. B* **2006**, *110* (14), 17866–17871.

(49) Rodriguez, J. A.; Hrbek, J.; Dvorak, J.; Jirsak, T.; Maiti, A. Interaction of sulfur with TiO2 (110). *Chem. Phys. Lett.* **2001**, *336*, 377–384.

(50) Murugesan, S.; Subramanian, V. Synthesis of bismuth titanate pyrochlore nanorods and its photocatalytic applications. *Chem. Commun.* **2009**, (34), 5109–5111.

(51) Perdew, J. P. Density Functional Theory and the Band-Gap Problem. *Int. J. Quantum Chem.* **1985**, 497–523.

(52) Perdew, J. P.; Burke, K.; Ernzerhof, M. Generalized gradient approximation made simple. *Phys. Rev. Lett.* **1996**, *77* (18), 3865–3868.

(53) Lin, Z. S.; Orlov, A.; Lambert, R. M.; Payne, M. C. New insights into the origin of visible light photocatalytic activity of nitrogen-doped and oxygen-deficient anatase TiO2. *J. Phys. Chem. B* **2005**, *109* (44), 20948–20952.

(54) Zhao, Z. Y.; Liu, Q. J. Designed highly effective photocatalyst of anatase TiO2 codoped with nitrogen and vanadium under visible-light irradiation using first-principles. *Catal. Lett.* **2008**, *124* (1−2), 111–117.

(55) Boschloo, G. K.; Goossens, A.; Schoonman, J. Photoelectrochemical study of thin anatase TiO2 films prepared by metallorganic chemical vapor deposition. *J. Electrochem. Soc.* **1997**, *144* (4), 1311–1317.

(56) Choi, W. Y.; Termin, A.; Hoffmann, M. R. Effects of Metal-Ion Dopants on the Photocatalytic Reactivity of Quantum-Sized Tio2 Particles. *Angew. Chem., Int. Ed. Engl.* **1994**, *33* (10), 1091–1092.

(57) Anpo, M.; Takeuchi, M.; Ikeue, K.; Dohshi, S. Design and development of titanium oxide photocatalysts operating under visible and UV light irradiation. The applications of metal ion-implantation techniques to semiconducting TiO2 and Ti/zeolite catalysts. *Curr. Opin. Solid State Mater. Sci.* **2002**, *6* (5), 381–388.

(58) Anpo, M.; Takeuchi, M. The design and development of highly reactive titanium oxide photocatalysts operating under visible light irradiation. *J. Catal.* **2003**, *216* (1−2), 505–516.

(59) Kavan, L.; Gratzel, M.; Gilbert, S. E.; Klemenz, C.; Scheel, H. J. Electrochemical and photoelectrochemical investigation of single-crystal anatase. *J. Am. Chem. Soc.* **1996**, *118* (28), 6716–6723.

(60) Mo, S. D.; Ching, W. Y. Electronic and Optical-Properties of 3 Phases of Titanium-Dioxide - Rutile, Anatase, and Brookite. *Phys. Rev. B* **1995**, *51* (19), 13023–13032.

(61) Zhang, L. W.; Fu, H. B.; Zhang, C.; Zhu, Y. F. Effects of Ta5+ substitution on the structure and photocatalytic behavior of the Ca2Nb2O7 photocatalyst. *J. Phys. Chem. C* **2008**, *112* (8), 3126–3133.

(62) Scaife, D. E. Oxide Semiconductors in Photoelectrochemical Conversion of Solar-Energy. *Sol. Energy* **1980**, *25* (1), 41–54.

(63) Cui, Y.; Du, H.; Wen, L. S. Doped-TiO2 Photocatalysts and Synthesis Methods to Prepare TiO2 Films. *J. Mater. Sci. Technol.* **2008**, *24* (5), 675–689.

(64) Fuerte, A.; Hernandez-Alonso, M. D.; Maira, A. J.; Martinez-Arias, A.; Fernandez-Garcia, M.; Conesa, J. C.; Soria, J. Visible light-activated nanosized doped-TiO2 photocatalysts. *Chem. Commun.* **2001**, (24), 2718–2719.

(65) Li, H. J.; Chen, G.; Li, Z. H.; Zhou, C. Synthesis and photocatalytic decomposition of water under visible light irradiation of La2Ti2-xCoxO7 with pyrochlore structure. *Acta Phys.-Chim. Sin.* **2007**, *23* (5), 761–764.

(66) Umebayashi, T.; Yamaki, T.; Itoh, H.; Asai, K. Analysis of electronic structures of 3d transition metal-doped TiO2 based on band calculations. *J. Phys. Chem. Solids* **2002**, *63* (10), 1909–1920.

(67) Mizushim, K.; Tanaka, M.; Iida, S. Energy-Levels of Iron Group Impurities in Tio2. *J. Phys. Soc. Jpn.* **1972**, *32* (6), 1519–&.

(68) Mizushima, K.; Tanaka, M.; Asai, A.; Iida, S.; Goodenough, J. B. Impurity Levels of Iron-Group Ions in Tio2 0.2. *J. Phys. Chem. Solids* **1979**, *40* (12), 1129–1140.

(69) Zou, Z. G.; Ye, J. H.; Arakawa, H. Photocatalytic water splitting into H-2 and/or O-2 under UV and visible light irradiation with a semiconductor photocatalyst. *Int. J. Hydrogen Energy* **2003**, *28* (6), 663–669.

(70) Luan, J. F.; Zou, Z. G.; Lu, M. H.; Zheng, S. R.; Chen, Y. F. Growth, structural and photophysical properties of Bi2GaTaO7. *J. Cryst. Growth* **2004**, *273* (1−2), 241–247.

(71) Wang, J. H.; Zou, Z. G.; Ye, J. H. Surface modification and photocatalytic activity of distorted pyrochlore-type Bi2M (M = In, Ga and Fe) TaO7 photocatalysts. *J. Phys. Chem. Solids* **2005**, *66* (2−4), 349–355.

(72) Zou, Z. G.; Ye, J. H.; Arakawa, H. Optical and structural properties of solid oxide photocatalyst Bi2FeNbO7. *J. Mater. Res.* **2001**, *16* (1), 35–37.

JP906252R